Received: 17 September 2024 | Accepted: 18 December 2024

DOI: 10.1002/ajb2.70014

RESEARCH ARTICLE

Botany

Gelatinous fibers develop asymmetrically to support bends and coils in common bean vines (*Phaseolus vulgaris*)

Joyce G. Onyenedum[1] | **Mariane S. Sousa-Baena**[2] | **Lena M. Hunt**[1] | **Angelique A. Acevedo**[1] | **Rosemary A. E. Glos**[3] | **Charles T. Anderson**[4]

[1]Department of Environmental Studies, New York University, New York, NY, USA

[2]Botany Department, Federal University of Rio Grande do Sul, Porto Alegre, Brazil

[3]Department of Ecology and Evolutionary Biology, University of Michigan, Ann Arbor, MI, USA

[4]Department of Biology and Center for Lignocellulose Structure and Formation, Pennsylvania State University, University Park, PA, USA

Correspondence

Joyce G. Onyenedum, 29 Washington Place Rm 150, New York, NY 10003, USA.
Email: jgo5750@nyu.edu

Abstract

Premise: Gelatinous (G)-fibers are specialized fibers that generate tensile force to bend and straighten many plant organs; this phenomenon has been intensively studied in tension wood of trees. Previous work has shown that G-fibers are common within the stems of twining vines, but we lack the spatiotemporal developmental data required to determine whether, or how, G-fibers contribute to the movement and/or stabilization of twining tissues.

Methods: We employed multiple histochemical approaches to characterize the formation and cell wall architecture of G-fibers in twining and shrub phenotypes of common bean across a developmental time series.

Results: Within an internode, G-fibers first formed asymmetrically via differentiation of pericyclic fibers on the concave side of an existing bend and later arose erratically from the vascular cambium. G-fibers were absent in immature and/or actively circumnutating internodes, thus validating previous reports that G-fibers are not involved in rapid dynamic movements. Instead, G-fibers formed in stationary internodes, where they developed (1) in an alternating asymmetric pattern, likely to support the posture maintenance of erect internodes at the base of twiners and throughout the length of shrubs or (2) on the concave side of twined internodes to stabilize their helical conformation.

Conclusions: Our spatiotemporal results indicate that common bean vines form G-fibers after an internode has fully elongated and becomes stationary, thus functioning to stabilize the posture of subtle bends and coil internodes. These results contribute to understanding how twining vines establish and maintain a grip on their host or supporting structure.

KEYWORDS

cell walls, coiled stems, common bean, development, Fabaceae, G-fibers, morphology, *Phaseolus vulgaris*, tensile fibers, twining, vines

Twining vines (hereafter "twiners") are by far the most common type of climbing plant (Acevedo-Rodríguez, 2015; Sperotto et al., 2020, 2023). In the United States, some introduced twiners are now aggressively invasive, such as kudzu (*Pueraria montana*), bittersweet (*Celastrus orbiculatus*), and wisteria (*Wisteria sinensis* and *W. floribunda*) (Forseth and Innis, 2004; Leicht-Young et al., 2007; Trusty et al., 2007). However, despite the prominence of these dynamic plants in many temperate and tropical ecosystems, there is still a lack of clarity regarding how twining vines establish and maintain their signature coiled stems. It has long been known that a twiner first engages in a searching motion (circumnutation) to locate a support or host (Darwin, 1865). Then, by tailoring its development in response to contact with the support (thigmotropism), a twiner will proceed to securely coil around it. Finally, a twiner must establish and maintain a tight grip to avoid sliding down to the ground (Matista and Silk, 1997).

But what morphological, anatomical, and biomechanical features support the helical posture of twiners? Previous work has demonstrated that slight increases in the stem radius through secondary growth and/or the development of stipules, petioles, or pulvini pinched between the vine and its support create localized tension and generate a squeezing force in some twiners (Isnard et al., 2009). An additional mechanism may be tensile gelatinous (G)-fibers, a common cell type in vines (Meloche et al., 2007; Bowling and Vaughn, 2009; Chery et al., 2021). Like ordinary fibers, G-fibers contain a primary wall and lignified secondary cell

wall layers, but G-fibers additionally contain an innermost thickened cell wall layer—the G-layer—composed of cellulose microfibrils embedded in a non-cellulosic matrix enriched in pectic rhamnogalacturonan I, arabinogalactan proteins, xyloglucans, and mannans (Nishikubo et al., 2007; Bowling and Vaughn, 2008; Gorshkova et al., 2015; Guedes et al., 2017; Kim and Daniel, 2019). The specialized composition of G-fibers facilitates the production of a strong tensile force (Gorshkova et al., 2018) that can bend a variety of plant organs including contractile roots (Zimmerman et al., 1968; Tomlinson et al., 2014) and tree trunks (Nugroho et al., 2012, 2018). G-fibers have independently evolved in a diversity of mobile plant organs, but their function in twining stems remains unclear (Meloche et al., 2007; Bowling and Vaughn, 2009; Chery et al., 2021).

The role of G-fibers has been best characterized in the tension wood of trees, which forms asymmetrically to "pull" leaning trunks back into a vertical conformation (Yoshida et al., 2000; Du and Yamamoto, 2007; Groover, 2016). Previous studies have found that many twiners have G-fibers in an array of stem tissues (Bowling and Vaughn, 2009; Chery et al., 2021), but it remains unknown when they form during the process of stem coiling. Here, to probe the relationship between G-fibers and twining, we analyzed the common bean, *Phaseolus vulgaris* L. (Fabaceae) and introduce it as an emergent experimental system for the study of vine development and anatomy. We employed time-lapse videography, immunohistochemistry, and detailed microscopy to characterize the development, morphology, and composition of G-fibers across developmental stages in both shrub and vining forms of common bean to determine how G-fibers contribute to twining movement and/or stem stabilization.

In this study, we identified five morphologically distinct stages in the growth of common bean and report that G-fibers are absent during initial twining movements but develop asymmetrically afterward to stabilize the curved position of internodes. G-fibers are not limited to dramatic coils in twiners but are also found in subtle bends of shorter internodes in both vining and shrub phenotypes, suggesting a role in posture maintenance.

MATERIALS AND METHODS

Plant cultivation

To compare G-fiber formation in common bean (*Phaseolus vulgaris*) plants with different growth habits were selected. We grew (1) recombinant inbred line (RIL) L88-57 (Frahm et al., 2004) and (2) 'Zenith' (Reg. No. CV307, PI 673047; Kelly et al., 2015), which were generously provided by Dr. Johnathan Lynch (Pennsylvania State University) and Dr. James D. Kelly (Michigan State University), respectively. L88-57 is the progeny of a cross between a type II upright short vine with limited branches and a type III vine with opportunistic branching (J. D. Kelly, personal communication; Frahm et al., 2004). Zenith is an upright shrub cultivar (Kelly et al., 2015). Seeds were germinated at Cornell University and New York University: Seeds were primed in an aqueous solution of 20% w/v polyethylene glycol 4000 (8074901000; Sigma Aldrich, Burlington, MA, USA) in the dark for 24 h, rinsed thoroughly, and incubated for 48 h in Petri dishes on water-saturated filter paper at room temperature (RT) on the laboratory bench.

L88-57 plants were grown under two conditions: (1) 130 μmol m^{-2} s^{-1} PAR to induce climbing or (2) 460 μmol m^{-2} s^{-1} PAR to induce the shrub phenotype. These two light conditions will be referred to as "low light" and "high light", respectively. The low light conditions included 12 h light with 130 μmol m^{-2} s^{-1} PAR, a 30-min ramp down, and 12 h dark, then a 30-min ramp up, with 50% RH in Environmental Growth Chamber (EGC) Models GR48 and SLR-90. Additional plants were grown in low light under the following conditions: 14 h light with 130 μmol m^{-2} s^{-1} PAR, 10 h dark, with 50% RH in the Cornell University Agricultural Experiment Station Guterman greenhouses (Ithaca, NY, USA). High light conditions included 12 h light at 460 μmol m^{-2} s^{-1} PAR with a 30-min ramp down, 12 h dark, then a 30-min ramp up, with 50% RH in the EGC chambers. 'Zenith' plants were grown in similar low light conditions as described above in EGC models GR48 and SLR-90. Plants were grown using Lambert LM-111 All Purpose Mix (Griffin Greenhouse Supplies, Tewksbury, MA, USA). Fertilizer (75 ppm of Jacks 15-5-15; JR Peters, Allentown, PA, USA) was applied as needed. All plants were potted in 10-cm plastic pots with 73 cm tall, 0.635 cm wide smooth plastic stakes (RooTrimmer, Nantong, China). Segment length was measured starting with the emergence of the cotyledons (only hypocotyl and epicotyl present), and each segment was measured again as new internodes emerged until a total of nine nodes with trifoliate leaves were present (the middle leaflet of the most apical trifoliate leaf reaching at least 0.3 cm long) (Appendix S1). For differences in stem segment lengths at maturity (nine emerged internodes), see Appendix S2.

Time-lapse videography

We used time-lapse videography to identify key stages in bean plant development and quantify the degree of circumnutation undergone by twining internodes. Raspberry Pi III (Cambridge, UK) computers were programmed with Raspberry Pi Camera V2 to image one frame every 20 min for 3 weeks. Plants were placed in front of a black velvet backdrop. We measured the diameter of the circumnutation revolution (roughly circular trajectory by the shoot tip) from maximum intensity projections of time-lapse images. Three time-lapse videos were used to obtain the diameter of circumnutation, the timing to complete one gyre, and one trajectory (i.e., revolution of the shoot) (Appendix S3).

An Apple iPhone 12 (Cupertino, CA, USA) was used in conjunction with the Lapse It application (Interactive Universe Creative Softwares Eireli, http://www.lapseit.com/) to capture one frame every 15 min during the stake removal assay (Appendix S4).

Developmental anatomy

To characterize the anatomy of G-fibers during the lifespan of twining and shrubby bean plants, we collected anatomical data at five developmental stages that we identified via consistent shifts in morphology: (1) erect seedling, (2) epicotyl bends, (3) regular circumnutation, (4) exaggerated circumnutation, and (5) twined. At each developmental stage, the middle portion of the hypocotyl, epicotyl, and each internode were sectioned and analyzed using the following protocol: Segments of the stem were fixed for 3 days in a solution of 5.5 parts 37% formalin (BP531-500; Fisher Scientific, Waltham, MA USA), 2.5 parts glacial acetic acid (BP2401-500; Fisher Scientific), 50 parts 70% ethanol, and 42 parts deionized water, then stored in 70% ethanol. Following transfer to ethanol, stem sections were cut by hand with an ASTRA01 razor blade (Gillette India, Rajasthan, India) from the middle of each internode. For hypocotyls, sections were cut closer to the epicotyl to obtain sections with stem-like, rather than root-like, anatomy. To differentiate lignified from nonlignified cellulosic cell walls, sections were double stained with safranin and astra blue (Bukatsch, 1972). Specifically, we used 1% w/v safranin-O (50-180-6544; Fisher Scientific) in 50% ethanol and 1% w/v astra blue (sc-214558; Santa Cruz Biotechnology, Dallas, TX, USA) in 50% ethanol in a 9:1 ratio. Sections were also separately stained with 2% w/v toluidine blue in water (Pradhan Mitra and Loqué, 2014). Stained sections were mounted in 50–100% glycerol, then viewed with bright-field optics using an Olympus BH2 microscope (Tokyo, Japan) and 10×/0.25 numerical aperture (NA), 20×/0.4 NA, or 40×/0.7 NA objective lenses. Images were taken using an AmScope MU 1000 digital camera (Irvine, CA, USA) mounted on the microscope. Additionally, unstained sections were imaged under UV light (405 nm excitation, 410–450 emission) using a Leica Stellaris 5 confocal microscope (Leica Microsystems, Wetzlar, Germany) with a 20×/0.75 NA objective lens. For developmental stages 1–3, we also immunolocalized developing G-fibers using an anti-RG-I primary antibody (LM5) and Alexa 488 goat anti-rat IgG Fab fragment secondary antibody as detailed in the next section.

Cell wall histology/immunohistochemistry

To localize cellulose/β-glucans in G-fibers using fluorescence microscopy, we stained sections with calcofluor white (#18909; Krackeler Scientific, Albany, NY, USA). Hand sections were stained in 50 µL aqueous 0.01% w/v calcofluor white and 50 µL of 10% w/v NaOH for 5 min at RT in darkness. Sections were rinsed in DI water and mounted in glycerol on glass slides. Sections were imaged with a 405 nm excitation laser and 405/60 nm emission window on the Stellaris 5 confocal microscope using a 20×/0.75 NA objective lens. To localize cellulose (Anderson et al., 2010), we stained sections with 0.01% (w/v) pontamine fast scarlet (S4B; #212490; Millipore Sigma, Milwaukee, WI, USA) in phosphate-buffered saline (PBS) for 40 min at RT in darkness, rinsed with PBS, then mounted in glycerol on glass slides. Sections were imaged with 532 nm excitation and at 595/40 nm emission window using a 63×/1.4 NA oil immersion objective lens with a 2× zoom factor.

To ensure that we were examining bona fide G-fibers, we used monoclonal antibodies to label cell wall components as follows: LM19 (ELD001; Kerafast, Shirley, MA, USA) and LM20 (ELD003, Kerafast) for pectin homogalacturonan (Verhertbruggen et al., 2009); LM5 (ELD007, Kerafast; Jones et al., 1997) and CCRC-M22 (Antibody kit SKCMA-AR1, CarboSource Services, Athens, GA, USA; (Pattathil et al., 2010) for rhamnogalacturonan-I; LM6 (ELD008, Kerafast; Willats et al., 1998) for arabinan side chain; LM10 (ELD016, Kerafast) and LM11 (ELD017, Kerafast) for xylan (McCartney et al., 2005); and LM15 (ELD013, Kerafast; Marcus et al., 2008) for xyloglucan. Cross sections were hand sliced with an Astra01 razor blade, blocked in PBS + 5% w/v nonfat Carnation powdered milk (Vevey, Switzerland) in 1.7 mL Eppendorf tubes for 40 min, then washed three times with PBS. Sections were incubated in primary antibody diluted 1:10 in PBS + 5% w/v nonfat Carnation powdered milk for 90 min at 20–22°C (RT), then washed three times in PBS. Sections were then incubated in secondary antibody diluted 1:100 in PBS + 5% (w/v) non-fat Carnation powdered milk for 90 min at 20–22°C (RT), then washed three times in PBS; Rhodamine Red-X (RRX) Goat Anti-Mouse IgG Fab fragment (115-296-003; Jackson Immunoresearch Laboratories, West Grove, PA, USA) was used for CCRC-M22 primary antibody, and Alexa 488 Goat anti-Rat IgG Fab fragment (A28175; Thermo Fisher Scientific) was used for all other primary antibodies. Negative controls lacking primary antibodies but incubated with secondary antibodies at RT were processed to observe any nonspecific fluorescence. Confocal images were collected on a Zeiss Cell Observer SD microscope with a Yokogawa CSU-X1 spinning disk head and a 63× or 100×/1.4 NA oil immersion objective lens. A 488 nm excitation laser and a 525/50 nm emission filter were used to detect epitopes tagged with Alexa 488 Goat anti-Rat IgG Fab fragment, and a 561 nm excitation laser and a 617/73 nm emission filter were used to image epitopes tagged with Rhodamine Red X (RRX) Goat Anti-Mouse IgG Fab fragment. For each antibody, two experiments were performed; each experiment comprised three cross sections of hypocotyls from three plants. See Appendices S5 and S6 for images of the immunolabeling.

Stake removal experiment

To systematically test whether G-fibers drive twining motions or whether they develop later to secure a helical posture, we designed an experiment to test the relative timing of coiling and G-layer deposition. Sixteen plants with five internodes were allowed to twine on a stake. For half of these plants, the stake was removed 48 h after the first gyre was established, then plants were grown without the stake until they reached 10 internodes; this group was called "stake removal early". For the other half of the plants, the stake was removed 96 h after the first gyre was established

(thus allowing more time for the plants to twine), then the plants were grown without the stake until they reached 10 internodes; this group was called "stake removal delayed". The internodes that twined (internodes 6–9) in both batches were sectioned to determine the presence/absence of G-fibers. An illustrative video can be found in Appendix S4.

Statistical analyses

Length measurements of each stem segment through five developmental stages was plotted (Appendix S1, accounting for plastochons 0 through 9) using the ggplot2 (Wickham, 2011) package in R (R Core Development Team, 2018). Internode lengths when plants had nine internodes were compared using a one-way ANOVA and Tukey's HSD post hoc test in R version 4.4.1 (R Core Team, 2018).

RESULTS

Common bean displays distinct morphological states across development

To understand the development of the twining habit in common bean, we studied internode elongation rates and time-lapse movies of recombinant inbred line (RIL) L88-57 (Frahm et al., 2004). Plants contacted the supports and began to climb them at nine internodes. By carefully studying development and tracking movements through time-lapse videos (Appendix S3), we identified five developmental stages in the establishment of the twining habit that each represent distinct morphological states of the stem (Figure 1).

In Stage 1, plants are erect seedlings with an aboveground hypocotyl, epicotyl, and two unifoliate seedling leaves (SI in Figure 1). In Stage 2, plants have a slightly bent epicotyl (S2 in Figure 1). In Stage 3, plants undergo regular circumnutation (typical of all plants) with a narrow trajectory, ≤9 cm in diameter (S3 in Figure 1). In Stage 4, the apical internodes rapidly elongate while performing exaggerated circumnutation, with a broad trajectory, ≥17 cm in diameter (S4 in Figure 1). Our measurement of circumnutation was within the 12–18 cm range reported for common bean by Millet et al. (1984). Each trajectory moved counterclockwise and took 1.67 h on average, close to the reported 1.57 h duration reported by Darwin (1875). Finally, if plants in Stage 4 were given a support stake, within 1.33 h, they completed their first gyre, thus beginning Stage 5 (S5 in Figure 1). Plants continued to coil around the support until the plant senesced. These five developmental stages are defined as follows: Stage 1, when the plant has only a pair of unifoliate seedling leaves; Stage 2, when three internodes with trifoliate leaves have emerged; Stage 3, when six internodes with trifoliate leaves have emerged; and Stages 4 and 5, when eight internodes with trifoliate leaves have emerged. Stage 5 is distinct from Stage 4 because the stem has twined. These stages approximately correspond to plastochrons 0, 3, 6, and 8, respectively.

Common bean has simple stem anatomy

During primary growth, the stems of common bean have the following tissues from the exterior inward: a single-layer epidermis, a multilayered cortex terminating in an endodermis (Figure 2A'), pericyclic fiber strands, vascular bundles in a ring, and central pith (Figure 2A). When a stem segment (hypocotyl,

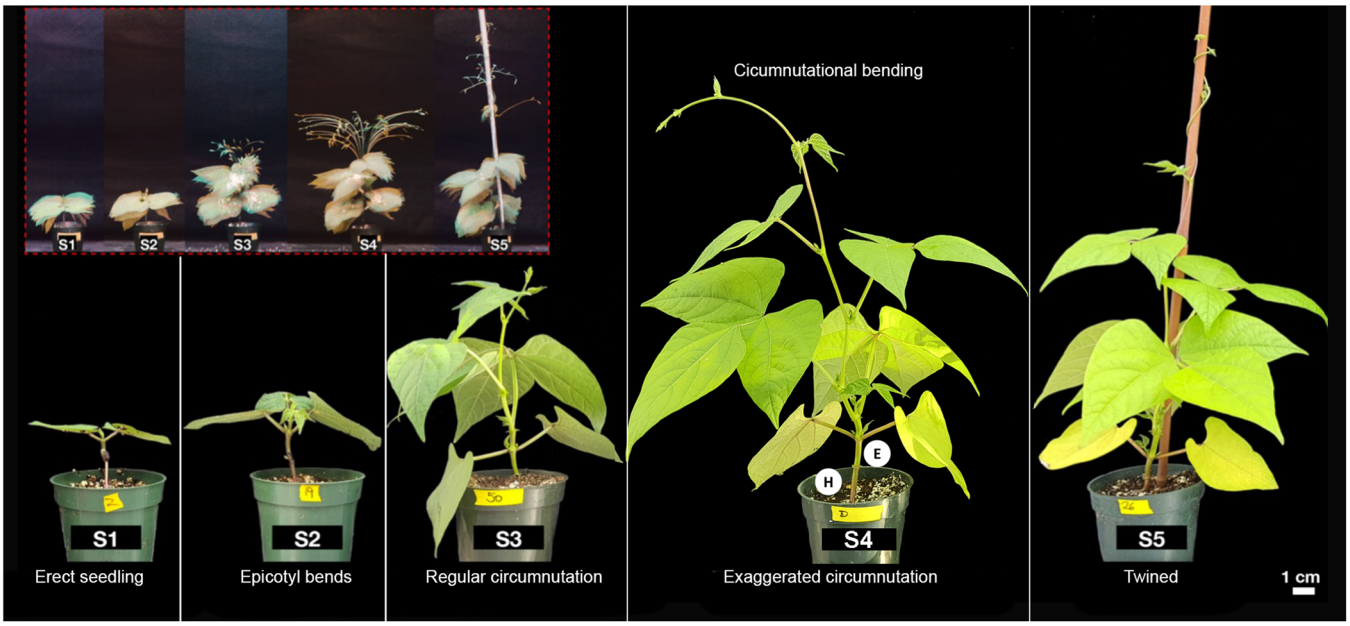

FIGURE 1 Five developmental stages (S1–S5) in the establishment of the twining habit in common bean (L88-57). Inset shows maximum intensity projections of time-lapse images of the same individual during the five developmental stages. H = hypocotyl, E = epicotyl.

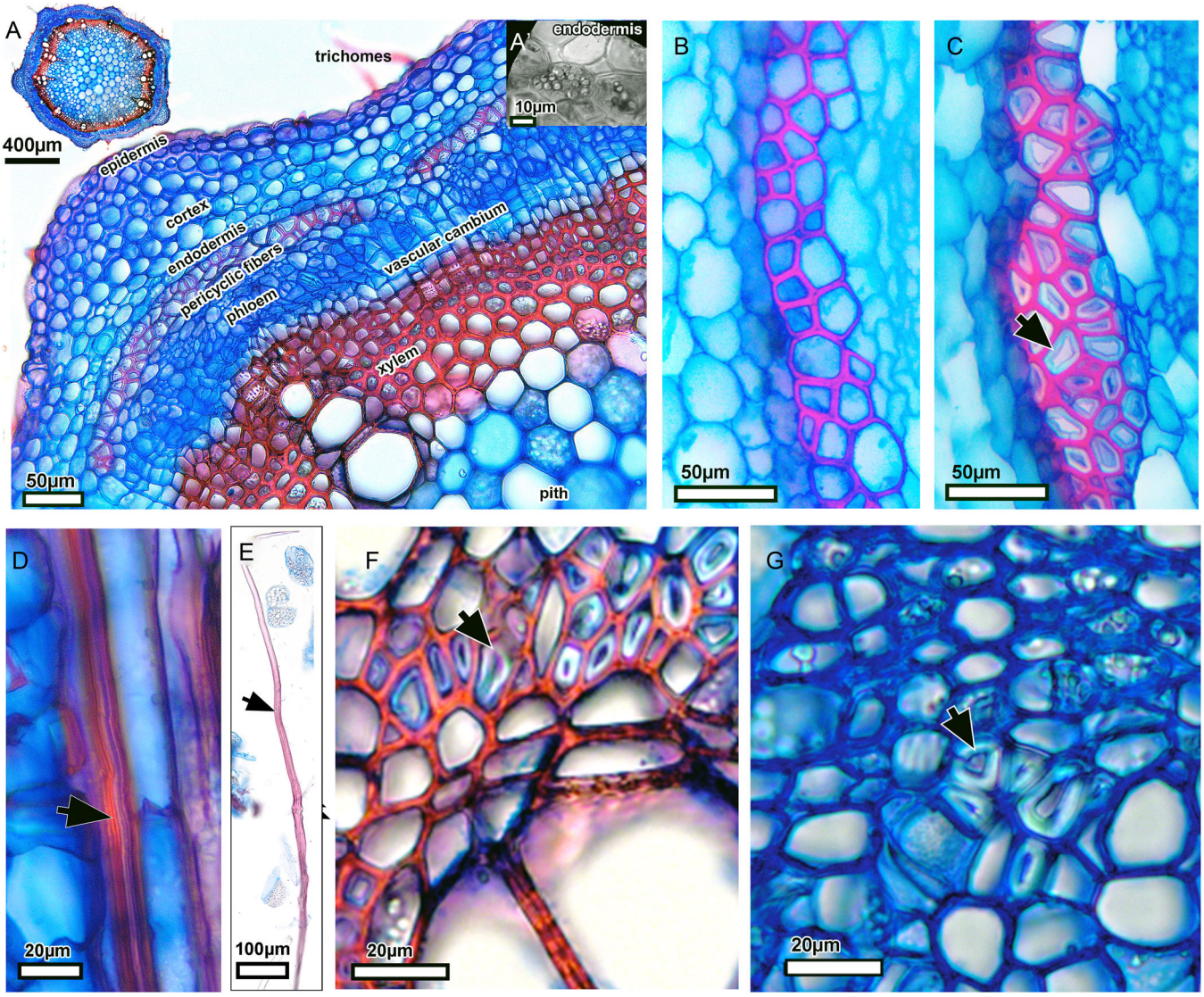

FIGURE 2 Light micrographs of stained cross sections of stems and G-fiber of common bean. All panel images are of Safranin + astra blue staining; blue (unlignified) and pink/red (lignified). Arrow points to G-layer within G-fibers. (A) General anatomy of young internode with key tissues labeled. Note the initiation of the vascular cambium, with secondary phloem immediately toward the exterior and secondary xylem to the interior. (A') Inset displays starch grains delimiting the endodermis. (B) Pericyclic fibers are present without G-layers. (C) Pericyclic fibers further differentiate into G-fibers by the production of a G-layer. (D) Contracted pericyclic G-fiber in situ. (E) Elongated pericyclic G-fiber from maceration of a mature internode reaching ~1.5 mm in length. (F, G) G-fibers in secondary tissues formed by the vascular cambium later in internode development. (F) Secondary xylem G-fibers. (G) Secondary phloem G-fibers.

epicotyl, or internode) had fully elongated and become stationary, G-fibers first appeared via differentiation of existing pericyclic fibers, which produced a G-layer (Figure 2B–E). As an internode matured and began to thicken via secondary growth, the vascular cambium produced G-fibers mainly in the secondary xylem (Figure 2F), and rarely in the secondary phloem (Figure 2G) in a seemingly erratic fashion.

G-fiber cell wall characteristics

The G-layer of G-fibers is often cited as being mostly cellulosic and devoid of lignin; however, recent reports indicate that lignification might be more widespread than previously expected (Roussel and Clair, 2015; Ghislain and Clair, 2017; Ghislain et al., 2019). We applied several approaches to assess the presence/absence of lignification of the G-layer. Double staining sections with safranin and astra blue (Bukatsch, 1972) typically yields a blue G-layer (unlignified) with red (lignified) outer S-layers (Figure 3A). However, we sometimes observed pink G-layers (Figure 3B), indicating lignification (Srebotnik and Messner, 1994; Vazquez-Cooz and Meyer, 2002). Staining with toluidine blue always resulted in blue (lignified) S-layers and a clear/faint blue G-layer, indicating a paucity of lignin (Figure 3C). UV-excitation at 405 nm of unstained samples yielded an autofluorescent signal indicative of phenolic compounds (possibly lignin) in the outer S-layers and the "Gn-layer"—

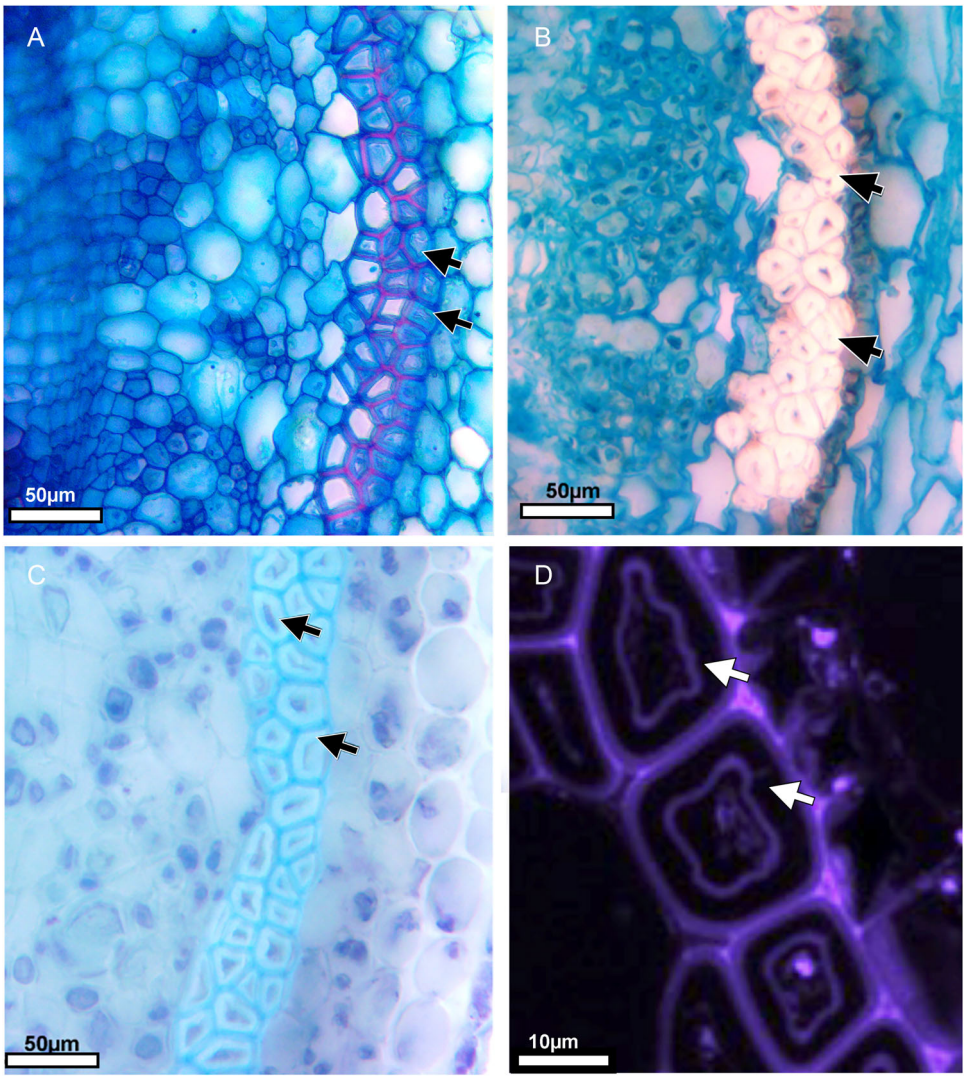

FIGURE 3 Results of differential staining of lignification of the G-layer. Arrows point to G-layer within G-fibers. (A) Safranin + astra blue sometimes yields blue (unlignified) G-layer or (B) pink G-layers (lignified). (C) Toluidine blue in water yields light blue to clear G-layers (unlignified). (D) UV autofluorescence indicates possible lignification only of the S-layers and innermost G-layer (Gn-layer), not the body of the G-layer itself.

the innermost region of the G-layer (Roach et al., 2011; Goudenhooft et al., 2019), but not in the main body of the G-layer (Figure 3D).

To further probe the cell wall epitope localization in common bean G-fibers, we next analyzed the localization of cellulose/β-glucans in developing bean stems. Staining with calcofluor white indicated cellulose/β-glucans in all cell wall layers of G-fibers (primary cell wall, secondary cell walls, and G-layer; Figure 4A). No signal was present in the negative controls (unstained sections) imaged under the same settings (Figure 4B). S4B staining for cellulose yielded a signal similar to that using calcofluor white, with signal on all cell wall layers of G-fibers (Figure 4C); the negative unstained controls had very faint signal on the S- and G-layers (Figure 4D).

Immunolabeling indicated that the G-layer contained the following pectin molecules: (1) rhamnogalacturonan I (Figure 5A) in the innermost face of the G-layer, the Gn-layer; (2) rhamnogalacturonan I with galactan side chains in the entire G-layer body (Figure 5B) and the outer walls of multilaminate G-layers (Figure 5C); and (3) low-methyl-esterified pectic homogalacturonan in the Gn-layer (Figure 5D). High-methyl-esterified pectic homogalacturonan was not detected in the G-layer, but detected in the primary cell wall/middle lamella (Figure 5E). Immunolabeling for (1→5)-α-L-arabinan pectin side chains was not detected in G-fibers (Figure 5F); however, ray parenchyma cells were labeled.

An antibody targeting the XXXG motif of xyloglucan (Figure 5G) strongly labeled the primary cell wall/middle lamella, with label at the interface of the secondary cell wall facing the G-layer and diffuse labeling in the G-layer itself. Antibodies targeting xylan did not label the primary cell walls/middle lamella; they labeled the secondary cell wall layers, and there was a faint signal on the G-layer itself (Figure 5H,I). Immunolabeling results

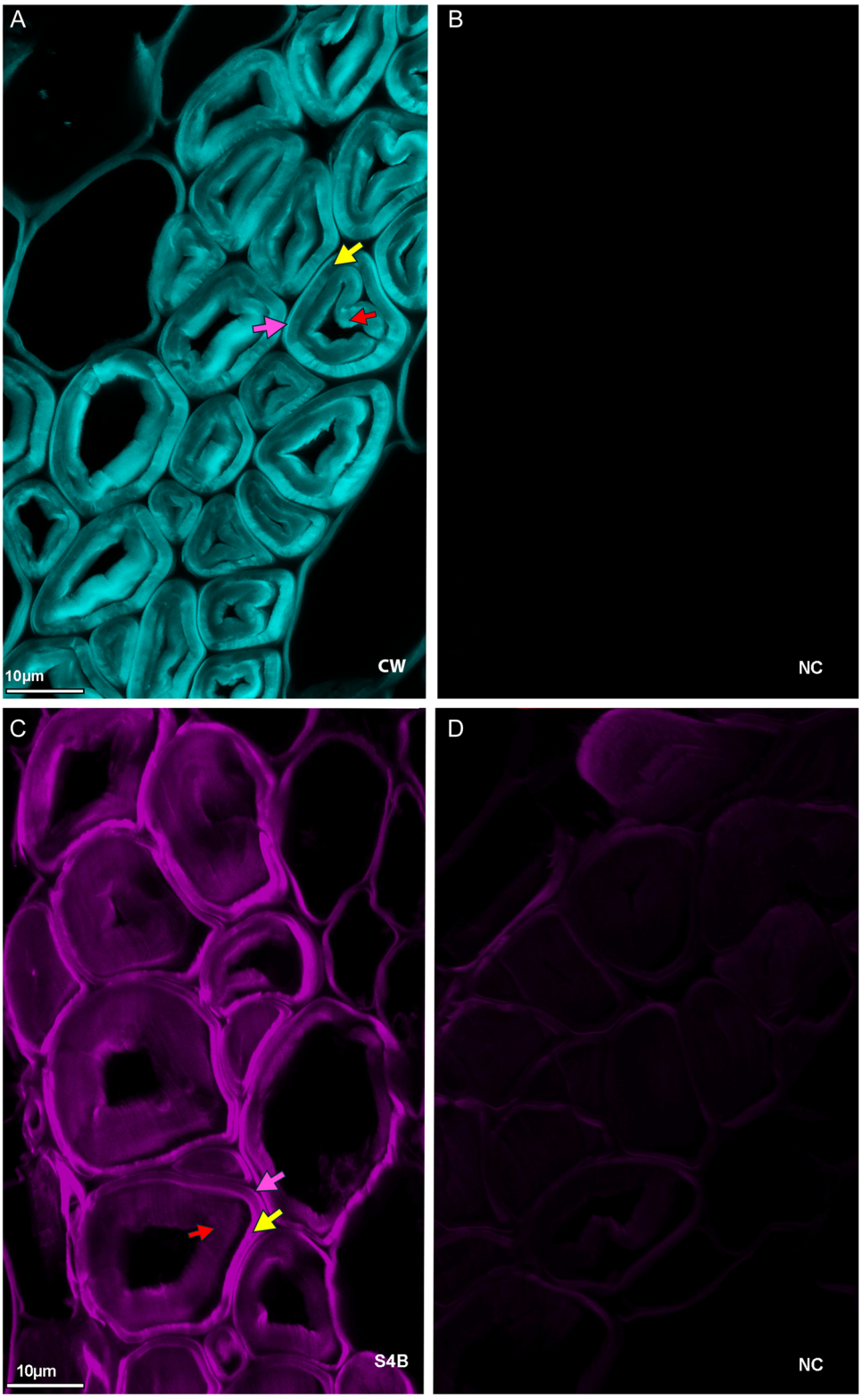

FIGURE 4 Fluorescence of histochemical stains for cellulose and/or β-glucans of G-fibers. (A, B) Images with 405 nm excitation and 405/60 nm emission window. (A) Calcofluor white (CW) staining reveals cellulose/β-glucan signal on pericyclic G-fibers; (B) negative control (NC) with autofluorescence. (C, D) Images with 532 excitation and 595/40 nm emission windows. (C) Cellulose staining with S4B; (D) negative control image with autofluorescence. Arrows: red = G-layer; yellow = secondary cell wall layers; pink = primary cell wall/middle lamella.

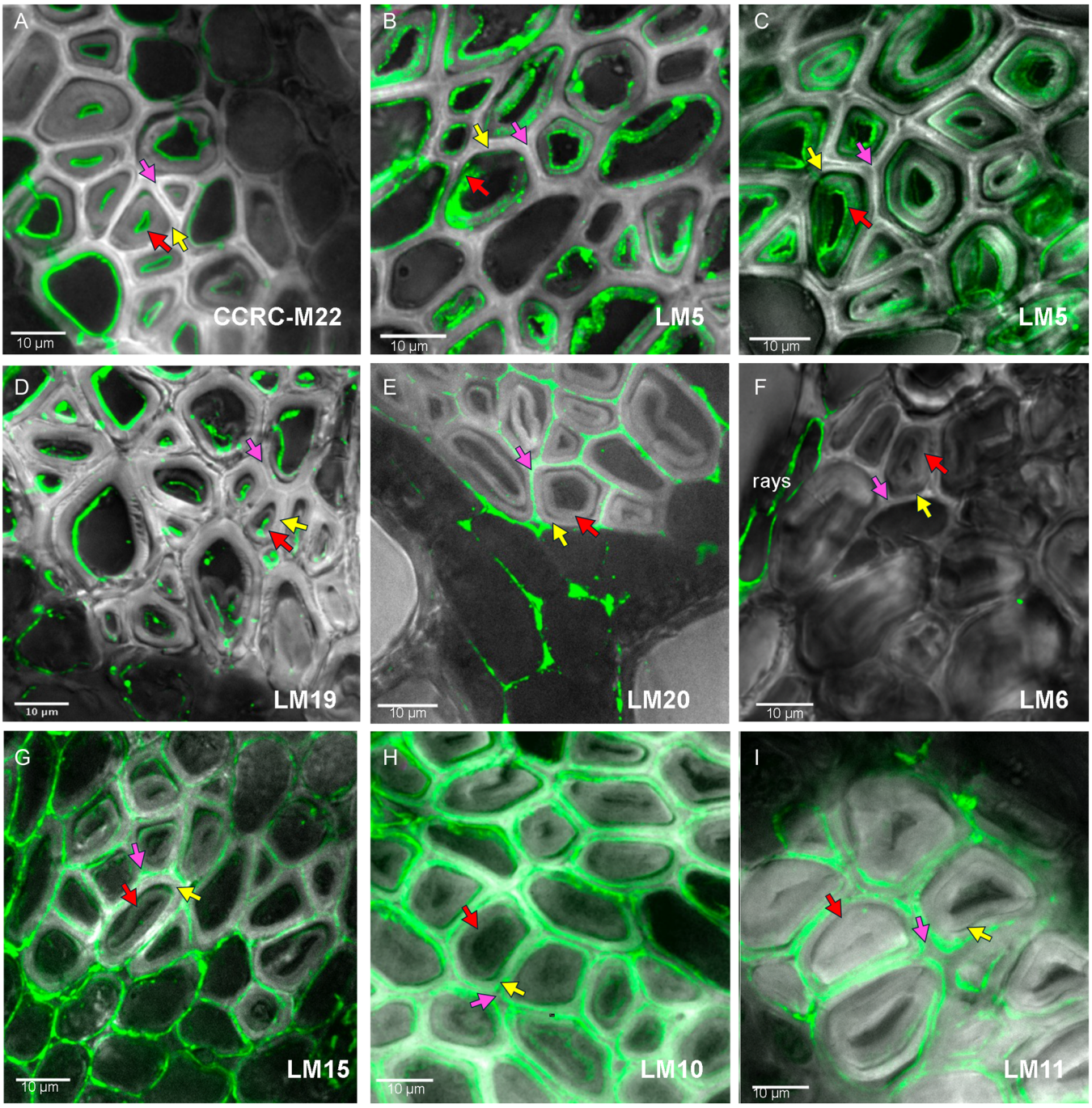

FIGURE 5 Immunolabeling with monoclonal antibodies to characterize the non-cellulosic matrix of G-fibers in hypocotyls 62 days after germination. Arrows: red = G-layer; yellow = secondary cell wall layers; pink arrow = primary cell wall/middle lamella. (A–F) Pectin immunolabeling results. (A) CCRC-M22 labels rhamnogalacturonan I (RG-I) on the innermost face of G-layer. No labeling on S-layers and primary cell wall/middle lamella. (B) LM5 labels galactan RG-I on the body of the G-layer, but not the S-layers or primary cell wall/middle lamella. (C) LM5 labels galactan RG-I on outer walls of multilaminate G-layer, but not the S-layers or primary cell wall/middle lamella. (D) LM19 labels low methyl-esterified homogalacturonan on the innermost face of the G-layer, but not the S-layers or primary cell wall/middle lamella. (E) LM20 labels high methyl-esterified homogalacturonan in the primary cell wall/middle lamella, but not the G-layer of S-layers. (F) LM6 labels (1-5)-α-L-arabinans labels of ray cells, but no cell wall layers of G-fibers. (G–I) Hemicellulose immunolabeling results. (G) LM15 labels XXXG motif of xyloglucan at the interface of the secondary cell wall facing the G-layer and primary cell wall/middle lamella with scattered distribution in the G-layer itself. (H, I) LM10 labels low substituted xylans in the secondary cell walls of G-layer. Faint label on some G-layers is present in the bottom right-hand corner in (I).

TABLE 1 Cell wall labeling patterns in common bean G-fibers.

Glycans	Antibodies	Localization	Primary cell wall/ middle lamella	Secondary cell wall layer 1/2	G-layer	
					Entire G-layer	Inner Gn-layer
Homogalacturonan	LM19	PCW-ML/G	X			X
	LM20	PCW-ML	X			
Rhamnogalacturonan type I	LM6	Not detected				
	LM5	**G**			**X**	**X**
	CCRC-M22	**G**				**X**
Xyloglucan	LM15	PCW-ML/S1-S2	X	X[a]	X[b]	
Xylan	LM10	S1-S2		X	X[b]	
	LM11	S1-S2		X		

Note: Antibodies in bold text specifically labeled the G-layer.

[a]Detected at the inner face of S2 of G-fibers.

[b]Faint detection.

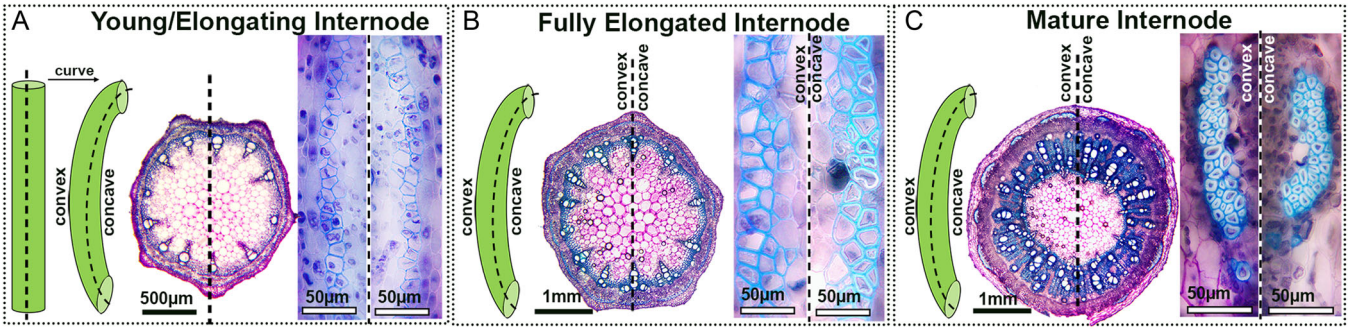

FIGURE 6 Stem shape, cross section, and image of differentiating G-fibers in young, maturing, and mature internodes. Dotted lines mark two halves of an internode. (A) Young/elongating internodes emerge straight then slightly bend; pericyclic fibers do not have G-layers (left and right insets). (B) Fully elongated internodes are bent; pericyclic fibers are differentiating into G-fibers only on the concave side (right insert). (C) Mature internodes are bent; pericyclic G-fibers are now present on both concave and convex sides (insets); note the presence of secondary growth at this stage.

are summarized in Table 1, and negative controls labeled with only secondary antibodies are shown in Appendices S5 and S6.

Straight basal vs. twined upper stem segments have contrasting distributions of G-fibers in common bean vines

To understand how G-fibers relate to plant movement, we tracked the spatiotemporal development of G-fibers throughout the five stages of twining development as described above. We focused on pericyclic G-fibers because their development temporally overlaps with the initial curvature and twining of any given internode (Figure 6A,B), whereas secondary xylem and phloem G-fibers are only found in mature internodes, well after a curved or coiled state has been established (Figure 6C).

In Stage 1 (erect seedlings), G-fibers were absent in both the hypocotyl and epicotyl (Figure 7A). In early Stage 2 (epicotyl bend), G-fibers developed on one side of the hypocotyl, while the epicotyl is slightly bent without G-fibers (Figure 7B). In late Stage 2, G-fibers formed on the concave surface (underside) of the bent epicotyl (Figure 7C). Overall, these seedlings had short internodes with G-fibers running on alternating sides of the plant from the hypocotyl to epicotyl (Figure 7C). During both Stages 3 (regular circumnutation) and 4 (exaggerated circumnutation), twiners are under a biomechanical state where the base of the plant remains stable and erect, while the apical internodes are moving (Appendix S3; Figures 1, 7D, 8A). The erect base—hypocotyl to internode 2—contained asymmetric G-fibers, on alternating sides of the stem (Figures 7D and 8B,B',C,C'). The dynamic apical internodes—internode 3 and above—did not have G-fibers (Figure 7D). In Stage 5, when plants had attached to a support, the apical internodes did not possess G-fibers yet as they were immature and only lightly attached to the support (Figure 8E,E'). However, in the internodes just below, we found G-fibers exclusively on the inside of the coil, following the path of a right-handed helix (Figure 8F–H).

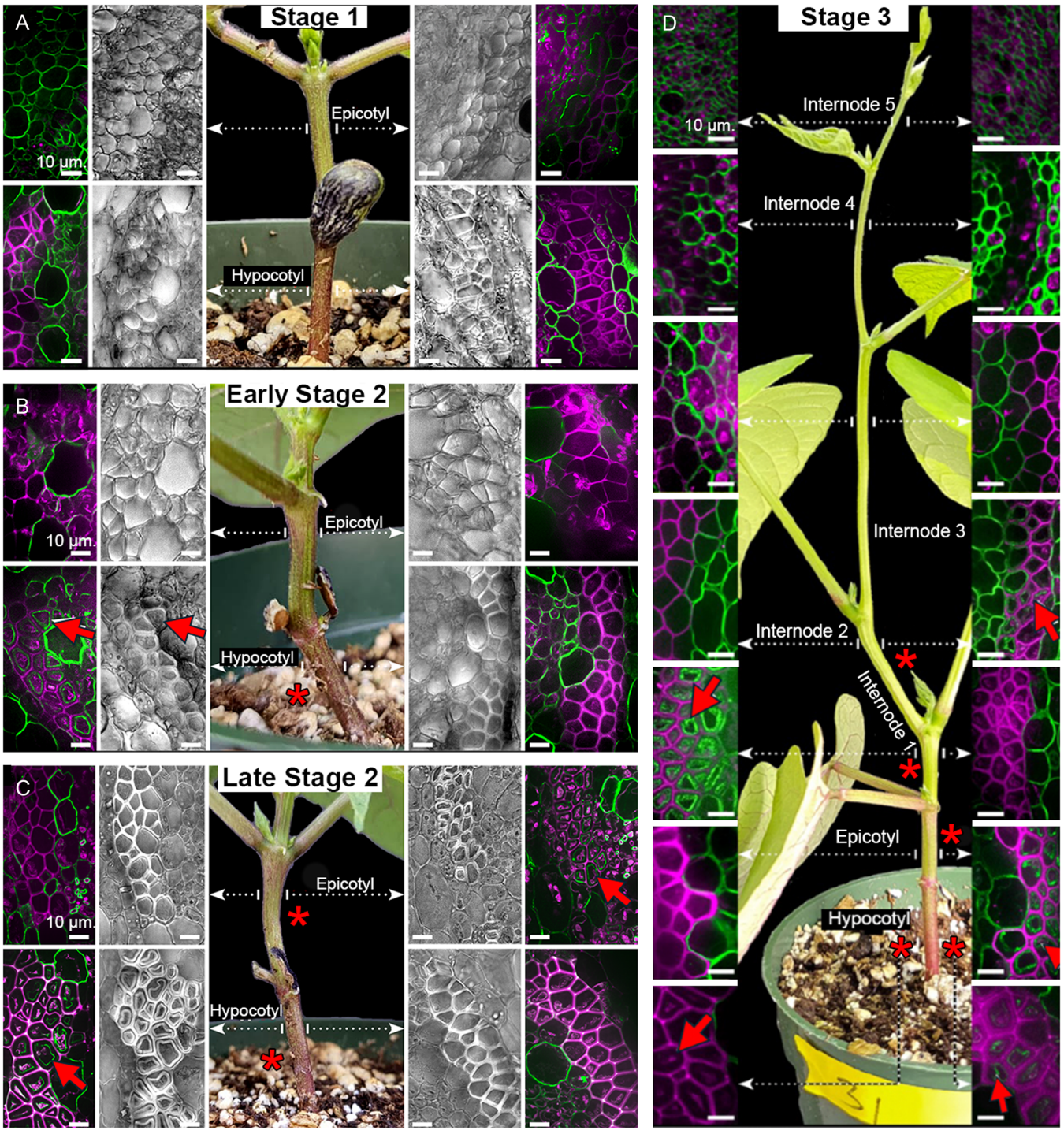

FIGURE 7 In Stages 1–3, pericyclic G-fibers develop asymmetrically in the hypocotyl, epicotyl, and internodes. (A–D) Confocal images are merged maximum projections z-stacks of autofluorescence excited with 405 nm laser (magenta) and rhamnogalacturonan-I (RG-I) labeled with LM5 primary antibody excited with 488 nm laser (green); grayscale images were viewed with bright-field optics. Red asterisk = the side of the internode with G-fibers. Red arrows = G-layers. (A) Stage 1. The epicotyl is straight and devoid of G-layers. (B) Early Stage 2. A subtle bend in the epicotyl appears, and G-fibers are on one side of the hypocotyl. No G-fibers are present in the epicotyl. (C) Late Stage 2. The subtle bend is reinforced by asymmetric production of G-fibers on the concave side of the epicotyl. (D) Stage 3 (regular circumnutation). Pericyclic fibers have differentiated asymmetrically, on alternating sides of the hypocotyl up to internode 2. Note that at this stage, G-fibers are on both sides of the hypocotyl; in the left image, the original G-fibers have matured, and in the right image are newly developed G-fibers with thin G-layers. G-fibers are absent from internode 3 upward; these internodes are immature and undergoing regular circumnutation. Scale bars = 10 µm.

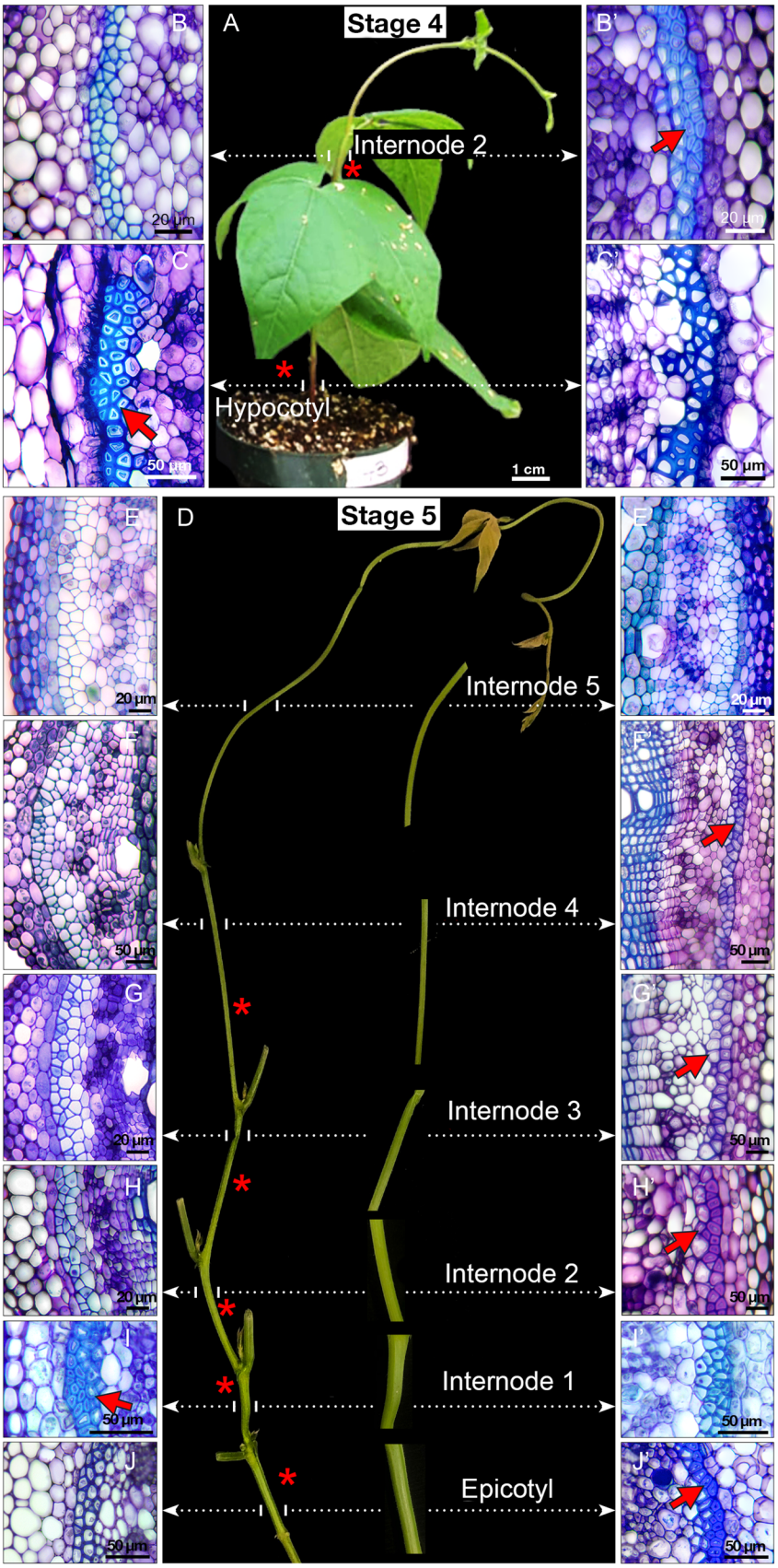

FIGURE 8 (See caption on next page).

G-layer deposition occurs after a gyre is established

We next performed an experiment to further test the relative timings of G-layer deposition and twining by removing the stake support from twined vines at two different times after the initiation of climbing. In the "stake removal early" group, plants were permitted to climb for 48 h (Figure 9A) before the stakes were removed. The previously twined internodes (6–8) re-straightened (Figure 9B, C) and resumed circumnutation, even re-twining again if the stake was replaced (Appendix S4). G-fibers were never present in previously twined internodes in this group (Figure 9D, E). By contrast, in the "stake removal delayed" group, plants were permitted to climb for 96 h (Figure 9F), before the stakes were removed. The previously twined internodes (6–8) maintained their coiled posture (Figure 9G, H), except for young, apical internodes (internode 9 in Figure 9G). G-fibers were abundantly present in the previously twined internodes in this group (Figure 9I, J), where plants remained in a twined conformation for longer (Figure 9). These coiled internodes have little to no secondary growth at this stage (see Figure 9, asterisk indicating secondary xylem vessels).

G-fiber development differs between shrub and twiner habits

Given the asymmetric appearance of G-fibers on the concave surface of both subtly curved and dramatically coiled internodes of twiners, we sought to investigate whether this is a vine-specific phenomenon or a feature inherent to the common bean species. Toward this aim, we grew twiner and shrub bean cultivars to 10 internodes (Figure 10A–C) to compare the presence/absence and localization of G-fibers along their stems. Internode elongation measurements and plant height are summarized in Appendices S1 and S2, respectively. G-fiber distribution schematics illustrating G-fiber distribution per individual samples are in Appendices S7–S9, and the summary results are outlined in Figure 10D–F.

All twiners in this study were grown under low light (130 μmol m^{-2} s^{-1}) (Figure 10A). Shrubs were grown in two ways: (1) Typically twining L88-57 plants were grown in high light (460 μmol m^{-2} s^{-1}), which repressed elongation and twining (Figure 10B), and (2) shrub cultivar Zenith plants were grown in low light (130 μmol m^{-2} s^{-1}) (Figure 10C). All Zenith and L88-57 shrubs grew erect and had shorter internodes than L88-57 twiners did (Appendices S1 and S2). The developmental progression of twiners and shrubs was similar until plants had seven internodes, at which point internode 3 elongated more in twiners than in shrubs (Appendix S1). Internodes 4–7 were the twining internodes in climbing L88-57 plants (Figure 10D). These internodes were significantly longer on twiners than on shrubs but statistically indistinguishable in the Zenith and L88-57 shrub habits (Appendices S1 and S2).

Like twiners, each internode in shrubs had a subtle curvature corresponding to a concave and convex side (Appendix S10), and surprisingly, both shrub habits produced G-fibers. As described above, twiners displayed an asymmetry of pericyclic G-fibers in the hypocotyl, epicotyl, and all internodes, whereby the stem base (hypocotyl to internode 2) displayed G-fibers on alternating sides, while the coiled internodes (internodes 3–5) displayed G-fibers on inside of the helix (Figure 10D). In contrast to the asymmetric pattern of pericyclic G-fibers in twiners, both shrub phenotypes had pericyclic G-fibers encircling the entire circumference of the stem base (hypocotyl, epicotyl, and internode 1 in Figure 10E, F). In shrubs, G-fibers were asymmetrically produced on alternating sides from internode 2 to 4, (Figure 10E, F), a similar pattern to the stem base of twiners.

DISCUSSION

In common bean, several factors contribute to this species being a successful twiner. First, it has trichomes along the stem axis (Figure 2A). In other climbers, such as *Ipomoea purpurea*, the coefficient of friction between the plant and its support is highest with hairy phenotypes (Silk and Holbrook, 2005). In different climbing plants, microspines (Lehnebach et al., 2022) or hook-like trichomes (Bauer et al., 2011) facilitate strong interlocking contact with a host plant or support. Second, common bean has stipules at the base of petioles (Acevedo-Rodríguez, 2020) an apparently common feature across twiners (Isnard and Silk, 2009; Isnard et al., 2009). Although easy to overlook, the expansion of stipules together with the stiffening of the stem is concomitant with an increase in squeezing forced in the twiner, *Dioscorea bulbifera* (Isnard et al., 2009). Twiners can maintain their helical posture under impressive gravitational loads. For example, an *I. purpurea* plant with two gyres and strong frictional coefficient of $\mu = 3$ requires a mass of 243 kg pulling at the base of the plant to induce

FIGURE 8 In Stages 4 and 5, G-fibers are present in stationary basal internodes; apical circumnutating internodes do not have G-fibers. Sections are stained with 2% w/v toluidine blue in water. Red asterisk = the side of the internode with G-fibers. Red arrows = G-layers. (A) Stage 4, exaggerated circumnutation occurs. Plant has five internodes and displays bending of the apical internodes that are circumnutating. (B-B') G-fibers are differentiated on concave side of internode 2. (C, C') G-fibers have differentiated on the concave side of the hypocotyl. (D) Stage 5. Twined plant unwound from the stake with leaves removed. G-fibers are on alternate sides of the stem from epicotyl to internode 2 (J, J'–H, H'). G-fibers are found on the same side in internodes 3 and 4 (G, G'–E, E') following the path of the helix. The most apical internodes (here, internodes 5–7) do not have yet G-fibers because they are immature and only lightly attached to the support.

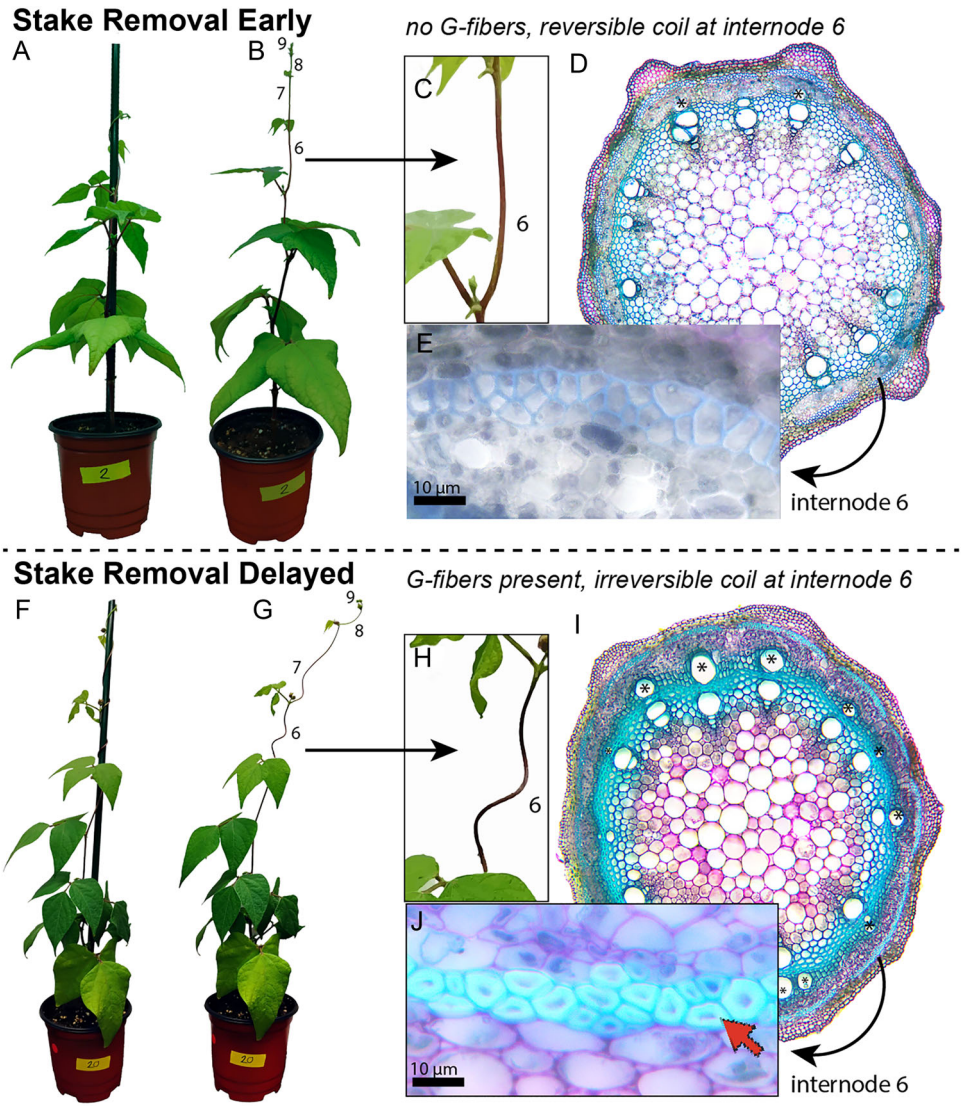

FIGURE 9 Pericyclic G-fibers do not initiate coiling and are not present in newly coiled internodes but develop later to maintain the coiled posture. (A–E) Stake removal early experiment. (A) Twiners were allowed to climb on a stake and complete the first gyre. (B) Stakes were removed 48 h later, then plants grew unsupported. (C) Close up showing that previously twined internodes re-straightened within 48 h without a stake. (D, E) Cross section of previously twined internode 6 showing the absence of pericyclic G-fibers. (F–I) Stake removal delayed experiment. (F) Twiners were allowed to climb on a stake. (G) Stakes were removed 96 h after the first gyre, then plants grew unsupported. (H) Close up showing that previously twined internodes maintain their coil posture when the stake was removed later. (I, J) Cross section of twined internode 6 showing the presence of pericyclic G-fibers. Sections were stained with 2% w/v toluidine blue. Red arrows = G-fibers. Asterisk = secondary xylem.

slipping (Silk and Holbrook, 2005). In addition to stipules, common bean plants also have anatomical features that place their stems in tension. In this paper, we investigated a third potential ingredient to common bean's success as climbers––the development of G-fibers, in both the pericyclic regions on the stem periphery (Figure 2B, C) and in the secondary vascular tissues (Figure 2F, G). Past studies have demonstrated that vines commonly have G-fibers within the tissue responsible for climbing, i.e., within the tendrils of tendril-climbing lianas and within the main stems of diverse twiners (Bowling and Vaughn, 2009), including common bean (Chery et al., 2021; Chernova et al., 2023).

Common bean has simple stem anatomy, except for the presence of G-fibers

The stem anatomy of common bean is typical of most seed plants, consisting of a eustele in primary growth followed by regular secondary growth (Figure 2A). Our anatomical interpretation of bean anatomy differs from that of Chernova et al. (2023) in one aspect: The innermost layer of the cortex has starch grains and can be interpreted as endodermis in bean (Figure 2A'). Thus, the cells just interior to this endodermis are the pericycle in accordance with other lineages (Tamaio et al., 2009; Cattai and de Menezes, 2010). Therefore, we here adopted the term "pericyclic fibers", instead of "bast fibers" or

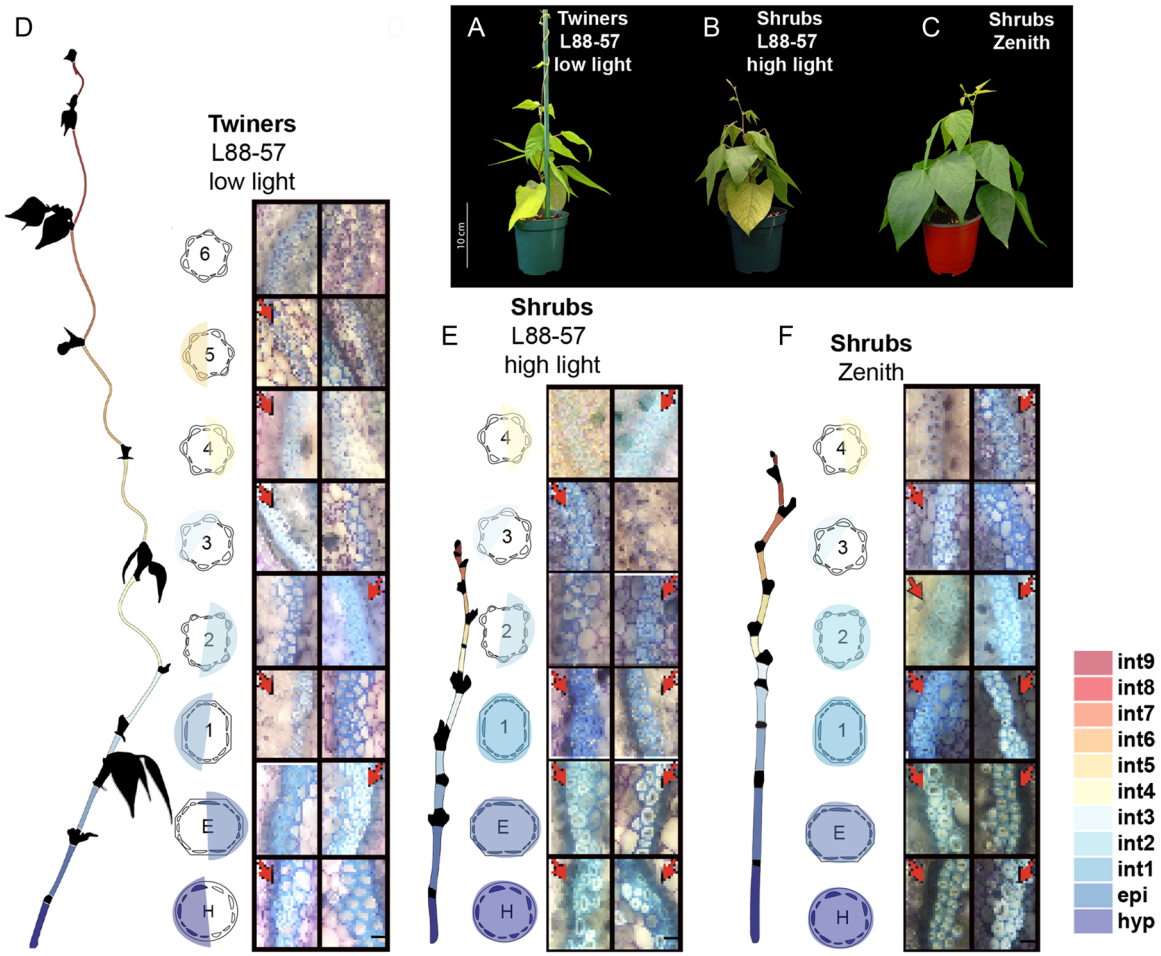

FIGURE 10 (A–C) Habit diversity of the common beans studied. (A) L88-57 grown as a twiner in low light (130 μmol m^{-2} s^{-1}); (B) L88-57 grown as a shrub in high light (460 μmol m^{-2} s^{-1}); (C) 'Zenith' grown as a shrub in low light. (D–F) G-fiber distribution in twiner vs. shrub common bean plants. Sections stained with 2% w/v toluidine blue in water. Red arrows = G-fibers. Representative stems of each phenotype were digitally traced from photographs to be in the same scale. Colors indicate the respective stem segment as indicated by the key in the lower right corner. Cross-section illustrations show localization of G-fibers around the circumference and are not to scale. (D) In unraveled L88-57 twiners, an asymmetrical G-fiber has differentiated on alternating sides of the hypocotyl up to internode 2. In twined internodes 3 to 5, G-fibers are localized along the inside of the coil. (E) L88-57 shrub. Pericyclic G-fibers are present in the entire circumference of the hypocotyl, epicotyl, and internode 1. Internodes 2 and 3 are relatively immature given the asymmetric G-fiber distribution. (F) 'Zenith'. Pericyclic G-fibers sheath the entire circumference of the hypocotyl, epicotyl, and internodes 1 and 2. Internodes 3 and 4 are relatively immature evident by the asymmetric G-fiber distribution. (D-F) Scale bar = 10 μm.

"primary phloem fibers" used by Chernova et al. (2023). Given the simplicity of common bean anatomy, the presence of tensile G-fibers stands out as a clear candidate to explain how these twiners form stable helical stems.

G-fibers in common bean are similar to those reported in other species, with possible traces of phenolic compounds

The G-fibers of common bean are similar in cell wall composition to other reported species with the G-layer composed of cellulose and pectins, with hemicelluloses on primary and/or secondary cell wall layers (Bowling and Vaughn, 2008; Mellerowicz and Gorshkova, 2012; Gorshkova et al., 2015; Guedes et al., 2017; Chernova et al., 2023). Chernova et al. (2023) isolated common bean G-fibers for wall compositional analyses and found that cellulose accounted for 74.7% of the dry mass of the cell walls and that galactose, galacturonic acid, arabinose, and rhamnose were dominant monosaccharides in the buffer-extractable fractions of common bean G-fibers. This particular wall composition is hypothesized to help generate strong tensile stress within the G-layer that has the capacity to bend an entire organ; however, there are various mechanistic explanations connecting cell wall architecture to whole organism form, and the matter remains unsettled (see reviews by (Mellerowicz and Gorshkova, 2012; Alméras and Clair, 2016; Gorshkova et al., 2018). The G-layer was once thought to be almost entirely cellulosic (Norberg and Meier, 1966); however, further investigations have revealed that G-layers in most species are ~75% cellulose, with the remainder being a non-cellulosic matrix of xyloglucans, pectins, mannans, and arabinogalactans (Nishikubo et al., 2007; Bowling and Vaughn, 2008; Gorshkova et al., 2015; Guedes et al., 2017; Kim and

Daniel, 2019). Of particular interest has been pectin rhamnogalacturonan-I (RG-I) (Figure 5A–C), a common feature in the G-layer of numerous species, which we also observed in this study (Bowling and Vaughn, 2008; Gorshkova et al., 2015; Guedes et al., 2017; Chernova et al., 2023). RG-I has even been proposed to be the source of tension in the G-layer, with molecules trapped between cellulose microfibrils, thus causing tension on these fibrils and the whole organ at large (Gorshkova et al., 2015; Mikshina et al., 2015).

In this study, our tests for the presence of lignin yielded conflicting results. For instance, histological staining (TBO and safranin and astra blue) revealed no lignin on the G-layer (Figure 3A–C); however, UV-induced autofluorescence indicated a faint pattern of possible lignification on the Gn-layer of an epicotyl cross section that matches the model in Figure 1E of Ghislain and Clair (2017) (Figure 3D). We infer that the G-layer in common bean is mostly devoid of lignin, with possible traces of lignin or another UV-fluorescent phenolic compound in the Gn-layer of more basal internodes. Variations in polymer composition and cellulose microfibril angle can optimize fibers to fulfill specific roles based on their position. For example, in a survey of fibers from different plants, high hemicellulose content was positively correlated with vibrational damping, while high microfibril angle and lignin content increased stiffness (Le Guen et al., 2016). Thus, there may be a difference in the nanoarchitecture of short basal G-fibers stabilizing small bends compared to G-fibers engaged in holding full coils in longer internodes. It is also possible that lignification occurs throughout the maturation of a G-layer, thus progressing towards a "stiff" state, contributing to the stability of the helix.

An alternative or perhaps concomitant mechanism that has been hypothesized to contribute to the tension generated in G-fibers involves xyloglucan and the action of xyloglucan endotransglycosylase/hydrolase (XET/XTH) enzymes. Xyloglucan is the most abundant component of the G-layer after cellulose (Mellerowicz et al., 2008). We detected the XXXG motif of xyloglucan sparsely in the G-layer itself, but strongly at the interface of the G-layer and the secondary cell wall using LM15 immunostaining (Figure 5G). These results correspond to findings in poplar G-fibers, where xyloglucan was most strongly detected on the secondary wall-facing surfaces of the G-layer, likely serving to tighten and secure the G-layer to its adjacent secondary cell wall (Baba et al., 2009). We note, however, that paucity of signal on the G-layer is common bean may be an artifact of tightly bound microfibrils in the G-layer preventing adequate penetration and visualization via antibody labeling. One hypothesis connecting xyloglucans to tensile stress is as follows: Well-hydrated G-layers press against the secondary cell walls, allowing XET/XTH enzymes to cleave and repair xyloglucan connections between cellulose fibrils, enabling the secondary wall to take on the tensile load of the G-fibers as they eventually lose water and undergo longitudinal shrinkage (Clair and Thibaut, 2001; Nishikubo et al., 2007). In transgenic poplar trees overexpressing XET, the excessive cleavage of xyloglucan connections results in stems that create a G-layer but fail to correct their posture when plants are placed on their side (Baba et al., 2009).

The spatiotemporal development of G-fibers suggests a role in posture maintenance for existing bends and coils

To understand the relationship between G-fiber development and twining, we tracked the spatiotemporal link between stages of twining (Figure 1) and fiber formation (Figures 7 and 8), which has also been done in studies of other systems. For instance, within the tendrils of cucumber vines, Gerbode et al. (2012) demonstrated that the tendril must first elongate, then G-fibers are clearly present when the tendril is attached in a coiled state. Bowling and Vaughn (2009) also reported that G-fibers were only observed after circumnutation had ceased and a twining stem and/or a coiling tendril arrived at the "setting stage" in various species. We found complementary results in common bean. Here we showed that G-fibers only appear after an internode ceases elongation and has coiled around a support, thus providing evidence that G-fibers function to reinforce existing bends. Within the model outlined by Isnard et al. (2009), we did not observe G-fibers in the "groping" zone, but it is unclear whether our stationary and fully elongated state is equivalent to the "gripping" or the "squeezing" stage without biomechanical measurements.

By contrast, Scher et al. (2001) found no temporal relationship between the lignification of fibers and increases in twining force in *Ipomoea purpurea*; thus, these fibers were postulated to facilitate ongoing increases to twining force after primary growth has ceased. Furthermore, our results contrast with the hypothesis laid out by Meloche et al. (2007), that G-fibers form concomitantly with the coiling of *Brunnichia ovata* tendrils, thus causing these tendrils to coil. We interpret their findings differently. The cortical band of fibers in *B. ovata* displays prominent labeling of anti-xylan antibodies during coiling; however, the G-layer is only present at day 5, when the tendril is already definitively coiled. This fiber differentiation is like the developmental trajectory of G-fibers in common bean, where the S1/S2 layers are laid down first, then the G-layer emerges post-attachment.

In common bean, we found that secondary xylem and phloem G-fibers only form in fully elongated internodes after pericyclic G-fibers have begun differentiating. The timing of secondary vascular G-fiber development suggests a supporting role in stiffening/tightening the grip, further contributing to a squeezing force (Putz and Holbrook, 1991) that was initiated by the pericyclic G-fibers. We found supporting evidence for this supposition in our stake removal experiments (Figure 9). Based on these data, the presence of pericyclic G-fiber appears to be a key determinant of whether a previously twined internode stem straightens and circumnutates when its support is removed or holds its coiled posture in the absence of a support (Appendix S4). At the stage sampled, minimal secondary growth was present in either stems that straightened or stems that held their posture (Figure 9). This result suggests that pericyclic G-fibers, rather than secondary growth, enable previously coiled internodes to remain in a helical state. Our findings agree with previous work demonstrating that increasing tensile force in twining *I. purpurea* was not related

to increases in radial growth. Moreover, our results support the hypothesis by Silk and Hubbard (1991, p. 605) that the anisotropic reinforcement of helical stems "might be provided by specialized fibers, such as sclerenchyma or collenchyma, which are known to be deposited toward the end of the period of longitudinal expansion".

The initial asymmetry associated with newly bent and coiled internodes is analogous to the tension–opposite wood division in trees (Groover, 2016), and the asymmetric contraction of G-fibers along the dorsiventral axis of cucumber tendrils (Gerbode et al., 2012; Fiorello et al., 2020). The distribution of G-fibers in common bean further mirrors patterns found in another member of Fabaceae, *Bauhinia glabra* (monkey ladder vine), where the asymmetrical distribution of G-fibers is associated with the undulating wood in vine stems; in this species, the concave surface of the stems produces more G-fibers than the convex does (Fisher and Blanco, 2014). However, in the case of *Bauhinia glabra*, the undulating curves were further reinforced by asymmetry in secondary growth, which was not observed, even after maturity, in the common beans sampled in this study (Stage 5, 8–10 internodes).

G-fibers are not exclusive to twiners

In addition to twiners, we also located G-fibers within the short and slightly curved internodes of common bean shrubs. Therefore, we conclude that G-fibers are not exclusively associated with the twining habit, but instead form constitutively within the species where they may serve to support subtle curves and more dramatic coils in common bean, depending on the habit. Shorter internodes of common bean shrubs showed more complete development of G-fibers around the full circumference of the pericycle, especially in basal internodes (Figure 10E, F). G-fiber distribution in shrubs (internode 2 and above) was like the basal internodes of twiners, i.e., present on alternating sides of the stem. However, in twiners, we found that this alternating pattern was absent in the apical mobile internodes. Instead, within the apical internodes of twiners, we found the pericyclic G-fibers along the concave side of a helical twined stem (Figure 8). We interpret this transition–from an alternating distribution along the stem base to a concentrated presence on the concave side of coiled internodes—as a structural shift. This shift likely reflects the change from a self-supporting seedling to a twined adult with twined internodes.

Common bean as a promising experimental system to study bending, twining, and coiling

Long studied as a global agricultural crop, common bean is now emerging as a versatile system for exploring fundamental developmental mechanisms linked to complex phenotypes on a multidisciplinary level, particularly those associated with growth habit and shifts between shrub and twiner. Common bean has the following qualities that make it well suited as an experimental system: (1) Plants can produce diverse and inducible growth habits through simple light manipulation (Van Dobben et al., 1981). (2) Plants reach vegetative maturity and display their growth habit as early as 4 weeks after germination (Gutierrez et al., 1994). (3) Depending on the variety, plants can have an early onset of flowering occurring as early as around 5 weeks after germination (Pekşen, 2007). (4) The capacity for self-pollination reduces the manual labor required to produce subsequent generations (plants can also outcross; Singh et al., 1991). (5) Lastly, given its status as a crop plant, four genomes have been published for common bean (https://phytozome-next.jgi.doe.gov/), providing fertile ground for elucidating the genetic basis of growth habit diversity in plants.

AUTHOR CONTRIBUTIONS

J.G.O. and C.T.A. conceived the project. J.G.O, M.S.S.B., A.A.A., R.A.E.G., and L.H. designed and performed the experiments and analyzed data. J.G.O. and A.A.A. wrote scripts. J.G.O. and M.S.S.B. wrote the initial article. All authors contributed to the final manuscript.

ACKNOWLEDGMENTS

The authors thank the Cornell Institute of Biotechnology's Imaging Facility for access to the Andor Revolution Spinning Disk Confocal Microscope (funded by NIH 1S10OD010605) and the kind reviewers of this manuscript whose helpful comments improved the quality of this work. This work was mainly supported by NSF CAREER award 2401675 to J.G.O. Parts of the growth and development and immunolocalization experiments were supported as part of The Center for Lignocellulose Structure and Formation, an Energy Frontier Research Center funded by the U.S. Department of Energy (DOE), Office of Science, Basic Energy Sciences (BES), under Award DE-SC0001090 to C.T.A.

CONFLICT OF INTEREST STATEMENT

The authors have no conflicts of interest.

DATA AVAILABILITY STATEMENT

Elongation measurements used to generate Appendix S1 and S2 are published on Zenodo (https://zenodo.org/records/14948189 and associated code available at http://github.com/angelique-acevedo/Common-Bean-Analysis).

ORCID

Joyce G. Onyenedum http://orcid.org/0000-0002-1047-9807
Mariane S. Sousa-Baena http://orcid.org/0000-0003-2080-1350
Lena M. Hunt http://orcid.org/0000-0002-7605-1379
Rosemary A. E. Glos http://orcid.org/0000-0002-5314-0846
Charles T. Anderson http://orcid.org/0000-0001-7481-3571

REFERENCES

Acevedo-Rodríguez, P. 2015. Lianas and climbing plants of the Neotropics. Website: https://naturalhistory.si.edu/research/botany/research/lianas-and-climbing-plants-neotropics [accessed 14 February 2024].

Acevedo-Rodríguez, P. 2020. Guide to the genera of lianas and climbing plants in the neotropics: Fabaceae.Website: https://naturalhistory.si.edu/sites/default/files/media/file/fabaceae.pdf [accessed 20 August 2024].

Alméras, T., and B. Clair. 2016. Critical review on the mechanisms of maturation stress generation in trees. *Journal of the Royal Society Interface* 13: 20160550.

Anderson, C. T., A. Carroll, L. Akhmetova, and C. Somerville. 2010. Real-time imaging of cellulose reorientation during cell wall expansion in Arabidopsis roots. *Plant Physiology* 152: 787–796.

Baba, K., Y. W. Park, T. Kaku, R. Kaida, M. Takeuchi, M. Yoshida, Y. Hosoo, et al. 2009. Xyloglucan for generating tensile stress to bend tree stem. *Molecular Plant* 2: 893–903.

Bauer, G., M.-C. Klein, S. N. Gorb, T. Speck, D. Voigt, and F. Gallenmüller. 2011. Always on the bright side: the climbing mechanism of *Galium aparine*. *Proceedings of the Royal Society, B, Biological Sciences* 278: 2233–2239.

Bowling, A. J., and K. C. Vaughn. 2009. Gelatinous fibers are widespread in coiling tendrils and twining vines. *American Journal of Botany* 96: 719–727.

Bowling, A. J., and K. C. Vaughn. 2008. Immunocytochemical characterization of tension wood: Gelatinous fibers contain more than just cellulose. *American Journal of Botany* 95: 655–663.

Bukatsch, F. 1972. Bermerkungen zur Doppelfärbung Astrablau-Safranin. *Mikrokosmos* 61: 255.

Cattai, M. B., and N. L. de Menezes. 2010. Primary and secondary thickening in the stem of *Cordyline fruticosa* (Agavaceae). *Anais da Academia Brasileira de Ciências* 82: 653–662.

Chernova, T., P. Mikshina, A. Petrova, N. Ibragimova, M. Ageeva, and T. Gorshkova. 2023. Rhamnogalacturonan I with β-(1,4)-galactan side chains as an ever-present component of tertiary cell wall of plant fibers. *International Journal of Molecular Sciences* 24: 17253.

Chery, J. G., R. A. E. Glos, and C. T. Anderson. 2021. Do woody vines use gelatinous fibers to climb? *New Phytologist* 233: 126–133.

Clair, B., and B. Thibaut. 2001. Shrinkage of the gelatinous layer of poplar and beech tension wood. *IAWA Journal* 22: 121–131.

Darwin, C. 1865. On the movements and babits of climbing plants. *Journal of the Linnean Society of London, Botany* 9: 1–118.

Darwin, C. 1875. The movements and habits of climbing plants, 2nd ed. John Murray, London, UK.

Du, S., and F. Yamamoto. 2007. An overview of the biology of reaction wood formation. *Journal of Integrative Plant Biology* 49: 131–143.

Fiorello, I., E. Del Dottore, F. Tramacere, and B. Mazzolai. 2020. Taking inspiration from climbing plants: methodologies and benchmarks—a review. *Bioinspiration & Biomimetics* 15: 031001.

Fisher, J. B., and M. A. Blanco. 2014. Gelatinous fibers and variant secondary growth related to stem undulation and contraction in a monkey ladder vine, *Bauhinia glabra* (Fabaceae). *American Journal of Botany* 101: 608–616.

Forseth, I. N., and A. F. Innis. 2004. Kudzu (*Pueraria montana*): History, physiology, and ecology combine to make a major ecosystem threat. *Critical Reviews in Plant Sciences* 23: 401–413.

Frahm, M. A., J. C. Rosas, N. Mayek-Pérez, E. López-Salinas, J. A. Acosta-Gallegos, and J. D. Kelly. 2004. Breeding beans for resistance to terminal drought in the lowland tropics. *Euphytica* 136: 223–232.

Gerbode, S. J., J. R. Puzey, A. G. McCormick, and L. Mahadevan. 2012. How the cucumber tendril coils and overwinds. *Science* 337: 1087–1091.

Ghislain, B., T. Alméras, J. Prunier, and B. Clair. 2019. Contributions of bark and tension wood and role of the G-layer lignification in the gravitropic movements of 21 tropical tree species. *Annals of Forest Science* 76: 1–13.

Ghislain, B., and B. Clair. 2017. Diversity in the organisation and lignification of tension wood fibre walls – a review. *IAWA Journal* 38: 245–265.

Gorshkova, T., T. Chernova, N. Mokshina, M. Ageeva, and P. Mikshina. 2018. Plant 'muscles': fibers with a tertiary cell wall. *New Phytologist* 218: 66–72.

Gorshkova, T., N. Mokshina, T. Chernova, N. Ibragimova, V. Salnikov, P. Mikshina, T. Tryfona, et al. 2015. Aspen tension wood fibers contain β-(1→4)-galactans and acidic arabinogalactans retained by cellulose microfibrils in gelatinous walls. *Plant Physiology* 169: 2048–2063.

Goudenhooft, C., A. Bourmaud, and C. Baley. 2019. Flax (*Linum usitatissimum* L.) fibers for composite reinforcement: exploring the link between plant growth, cell walls development, and fiber properties. *Frontiers in Plant Science* 10: 1–23.

Groover, A. 2016. Gravitropisms and reaction woods of forest trees – evolution, functions and mechanisms. *New Phytologist* 211: 790–802.

Guedes, F. T. P., F. Laurans, B. Quemener, C. Assor, V. Lainé-Prade, N. Boizot, J. Vigouroux, et al. 2017. Non-cellulosic polysaccharide distribution during G-layer formation in poplar tension wood fibers: abundance of rhamnogalacturonan I and arabinogalactan proteins but no evidence of xyloglucan. *Planta* 246: 857–878.

Gutierrez, A. P., E. J. Mariot, and C. S. W. Riddle. 1994. A model of bean (*Phaseolus vulgaris* L.) growth types I–III: factors affecting yield. *Agricultural Systems* 44: 35–63.

Isnard, S., A. R. Cobb, N. M. Holbrook, M. Zwieniecki, and J. Dumais. 2009. Tensioning the helix: a mechanism for force generation in twining plants. *Proceedings of the Royal Society, B, Biological Sciences* 276: 2643–2650.

Isnard, S., and W. K. Silk. 2009. Moving with climbing plants from Charles Darwin's time into the 21st century. *American Journal of Botany* 96: 1205–1221.

Jones, L., C. B. Seymour, and J. P. Knox. 1997. Localization of pectic galactan in tomato cell walls using a monoclonal antibody specific to (1→4)-*β*-d-galactan. *Plant Physiology* 113: 1405–1412.

Kelly, J. D., G. V. Varner, K. A. Cichy, and E. M. Wright. 2015. Registration of 'Zenith' black bean. *Journal of Plant Registrations* 9: 15–20.

Kim, J. S., and G. Daniel. 2019. Xyloglucans in the G-layer. *BioResources* 14: 7675–7686.

Le Guen, M.-J., R. H. Newman, A. Fernyhough, S. J. Hill, and M. P. Staiger. 2016. Correlations between the physiochemical characteristics of plant fibres and their mechanical properties. In R. Fangueiro and S. Rana [eds.], Natural fibres: Advances in science and technology towards industrial applications: from science to market, 35–47. Springer, Dordrecht, Netherlands.

Lehnebach, R., C. Paul-Victor, E. Courric, and N. P. Rowe. 2022. Microspines in tropical climbing plants: a small-scale fix for life in an obstacle course. *Journal of Experimental Botany* 73: 5650–5670.

Leicht-Young, S. A., J. A. Silander, and A. M. Latimer. 2007. Comparative performance of invasive and native *Celastrus* species across environmental gradients. *Oecologia* 154: 273–282.

Marcus, S. E., Y. Verhertbruggen, C. Hervé, J. J. Ordaz-Ortiz, V. Farkas, H. L. Pedersen, W. G. Willats, and J. P. Knox. 2008. Pectic homogalacturonan masks abundant sets of xyloglucan epitopes in plant cell walls. *BMC Plant Biology* 8: 60.

Matista, A. A., and W. K. Silk. 1997. An electronic device for continuous, in vivo measurement of forces exerted by twining vines. *American Journal of Botany* 84: 1164–1168.

McCartney, L., S. E. Marcus, and J. P. Knox. 2005. Monoclonal antibodies to plant cell wall xylans and arabinoxylans. *Journal of Histochemistry and Cytochemistry* 53: 543–546.

Mellerowicz, E. J., and T. A. Gorshkova. 2012. Tensional stress generation in gelatinous fibres: a review and possible mechanism based on cell-wall structure and composition. *Journal of Experimental Botany* 63: 551–565.

Mellerowicz, E. J., P. Immerzeel, and T. Hayashi. 2008. Xyloglucan: the molecular muscle of trees. *Annals of Botany* 102: 659–665.

Meloche, C. G., J. P. Knox, and K. C. Vaughn. 2007. A cortical band of gelatinous fibers causes the coiling of redvine tendrils: a model based upon cytochemical and immunocytochemical studies. *Planta* 225: 485–498.

Mikshina, P. V., A. A. Petrova, D. A. Faizullin, Yu. F. Zuev, and T. A. Gorshkova. 2015. Tissue-specific rhamnogalacturonan I forms the gel with hyperelastic properties. *Biochemistry* 80: 915–924.

Millet, B., D. Melin, B. Bonnet, C. A. Ibrahim, and J. Mercier. 1984. Rhythmic circumnutation movement of the shoots in *Phaseolus vulgaris* L. *Chronobiology International* 1: 11–19.

Nishikubo, N., T. Awano, A. Banasiak, V. Bourquin, F. Ibatullin, R. Funada, H. Brumer, et al. 2007. Xyloglucan *endo*-transglycosylase (XET) functions in gelatinous layers of tension wood fibers in poplar—A glimpse into the mechanism of the balancing act of trees. *Plant and Cell Physiology* 48: 843–855.

Norberg, P. H., and H. Meier. 1966. Physical and chemical properties of the gelatinous layer in tension wood fibres of aspen (*Populus tremula* L.). *Holzforschung* 20: 174–178.

Nugroho, W. D., S. Nakaba, Y. Yamagishi, S. Begum, M. H. Rahman, K. Kudo, S. N. Marsoem, and R. Funada. 2018. Stem gravitropism and tension wood formation in *Acacia mangium* seedlings inclined at various angles. *Annals of Botany* 122: 87–94.

Nugroho, W. D., Y. Yamagishi, S. Nakaba, S. Fukuhara, S. Begum, S. N. Marsoem, J. H. Ko, et al. 2012. Gibberellin is required for the formation of tension wood and stem gravitropism in *Acacia mangium* seedlings. *Annals of Botany* 110: 887–895.

Pattathil, S., U. Avci, D. Baldwin, A. G. Swennes, J. A. McGill, Z. Popper, T. Bootten, et al. 2010. A comprehensive toolkit of plant cell wall glycan-directed monoclonal antibodies. *Plant Physiology* 153: 514–525.

Peksen, E. 2007. Dynamics of flowering appearance, flowering, pod and seed setting performance and their relations to seed yield in common bean (*Phaseolus vulgaris* L.). *Pakistan Journal of Botany* 39: 485–496.

Pradhan Mitra, P., and D. Loqué. 2014. Histochemical staining of *Arabidopsis thaliana* secondary cell wall elements. *Journal of Visualized Experiments* 87: e51381.

Putz, F. E., and N. M. Holbrook. 1991. Biomechanical studies in vines. In F. E. Putz and H. A. Mooney [eds.], Biomechanical studies in vines, 73–97. Cambridge University Press, Cambridge, UK.

R Core Team. 2018. R: A language and environment for statistical computing. R Foundation for Statistical Computing, Vienna, Austria. Website: https://www.R-project.org/

Roach, M. J., N. Y. Mokshina, A. Badhan, A. V. Snegireva, N. Hobson, M. K. Deyholos, and T. A. Gorshkova. 2011. Development of cellulosic secondary walls in flax fibers requires β-galactosidase. *Plant Physiology* 156: 1351–1363.

Roussel, J.-R., and B. Clair. 2015. Evidence of the late lignification of the G-layer in *Simarouba* tension wood, to assist understanding how non-G-layer species produce tensile stress. *Tree Physiology* 35: 1366–1377.

Scher, J. L., N. M. Holbrook, and W. K. Silk. 2001. Temporal and spatial patterns of twining force and lignification in stems of *Ipomoea purpurea*. *Planta* 213: 192–198.

Silk, W. K., and N. M. Holbrook. 2005. The importance of frictional interactions in maintaining the stability of the twining habit. *American Journal of Botany* 92: 1820–1826.

Silk, W. K., and M. Hubbard. 1991. Axial forces and normal distributed loads in twining stems of morning glory. *Journal of Biomechanics* 24: 599–606.

Singh, S. P., P. Gepts, and D. G. Debouck. 1991. Races of common bean (*Phaseolus vulgaris*, Fabaceae). *Economic Botany* 45: 379–396.

Sperotto, P., P. Acevedo-Rodríguez, T. N. C. Vasconcelos, and N. Roque. 2020. Towards a standardization of terminology of the climbing habit in plants. *Botanical Review* 86: 180–210.

Sperotto, P., N. Roque, P. Acevedo-Rodríguez, and T. Vasconcelos. 2023. Climbing mechanisms and the diversification of neotropical climbing plants across time and space. *New Phytologist* 240: 1561–1573.

Srebotnik, E., and K. Messner. 1994. A simple method that uses differential staining and light microscopy to assess the selectivity of wood delignification by white rot fungi. *Applied and Environmental Microbiology* 60: 1383–1386.

Tamaio, N., R. Vieira, and V. Angyalossy. 2009. Origin of successive cambia on stem in three species of Menispermaceae. *Brazilian Journal of Botany* 4: 839–848.

Tomlinson, P. B., T. M. Magellan, and M. P. Griffith. 2014. Root contraction in *Cycas* and *Zamia* (Cycadales) determined by gelatinous fibers. *American Journal of Botany* 101: 1275–1285.

Trusty, J. L., L. R. Goertzen, W. C. Zipperer, and B. G. Lockaby. 2007. Invasive *Wisteria* in the Southeastern United States: genetic diversity, hybridization and the role of urban centers. *Urban Ecosystems* 10: 379–395.

Van Dobben, W. H., A. Van Ast, and W. J. Corré. 1981. The influence of light intensity on morphology and growth rate of bean seedlings. *Acta Botanica Neerlandica* 30 (1/2): 33–45.

Vazquez-Cooz, I., and R. W. Meyer. 2002. A differential staining method to identify lignified and unlignified tissues. *Biotechnic & Histochemistry* 77: 277–282.

Verhertbruggen, Y., S. E. Marcus, A. Haeger, J. J. Ordaz-Ortiz, and J. P. Knox. 2009. An extended set of monoclonal antibodies to pectic homogalacturonan. *Carbohydrate Research* 344: 1858–1862.

Wickham, H. 2011. ggplot2. *Wiley Interdisciplinary Reviews: Computational Statistics* 3: 180–185.

Willats, W. G. T., S. E. Marcus, and J. P. Knox. 1998. Generation of a monoclonal antibody specific to (1→5)-l-arabinan. *Carbohudrate Research* 308: 149–152.

Yoshida, M., T. Okuda, and T. Okuyama. 2000. Tension wood and growth stress induced by artificial inclination in *Liriodendron tulipifera* Linn. and *Prunus spachiana* Kitamura f. *ascendens* Kitamura. *Annals of Forest Science* 57: 739–746.

Zimmerman, M. H., A. B. Wadrop, and P. B. Tomlinson. 1968. Tension wood in aerial roots of *Ficus benjamin*a L. *Wood Science and Technology* 2: 95–104.

SUPPORTING INFORMATION

Additional supporting information can be found online in the Supporting Information section at the end of this article.

Appendix S1. Total height and hypocotyl, epicotyl, and internode elongation of L88-57 low light twiners, L88-57 high light shrubs, and Zenith shrubs over stages of development.

Appendix S2. Stem segments and total height of twiner versus shrub morphology plants at maturity.

Appendix S3. Movie of twiner, L88-57, and shrub Zenith.

Appendix S4. Movie of stake removal assay.

Appendix S5. Immunolabeling of xylary G-fibers I (CCRC-M22, LM19, LM20).

Appendix S6. Immunolabeling of xylary G-fibers II (LM6, LM10, LM11, LM15).

Appendix S7. G-fiber positional data along the stems of L88-57 twiners.

Appendix S8. G-fiber positional data along the stems of L88-57 shrubs.

Appendix S9. G-fiber positional data along the stems of Zenith.

Appendix S10. Subtle curvature of an internode in L88-57 shrub.

How to cite this article: Onyenedum, J. G., M. S. Sousa-Baena, L. M. Hunt, A. A. Acevedo, R. A. E. Glos, and C. T. Anderson. 2025. Gelatinous fibers develop asymmetrically to support bends and coils in common bean vines (*Phaseolus vulgaris*). *American Journal of Botany* 112(3): e70014. https://doi.org/10.1002/ajb2.70014